Journal of Membrane Science 453 (2014) 603–613

Contents lists available at ScienceDirect

Journal of Membrane Science

journal homepage: www.elsevier.com/locate/memsci

Improving the mechanical strength and gas separation performance of CMS membranes by simply sintering treatment of α-Al_2O_3 support

Ming-Yen Wey [a], Hui-Hsin Tseng [b,c,*], Chian-kai Chiang [b,c]

[a] Department of Environmental Engineering, National Chung Hsing University, No. 250, Guoguang Road, South District, Taichung City, Taiwan, ROC
[b] School of Occupational Safety and Health, Chung Shan Medical University, No.110, Sec. 1, Jianguo N. Road, Taichung City, Taiwan, ROC
[c] Department of Occupational Medicine, Chung Shan Medical University Hospital, No.110, Sec. 1, Jianguo N. Road, Taichung City, Taiwan, ROC

ARTICLE INFO

Article history:
Received 5 September 2013
Received in revised form
25 October 2013
Accepted 22 November 2013
Available online 11 December 2013

Keywords:
Carbon membrane
Gas separation
Mechanical strength
Substrate
Sintering

ABSTRACT

Asymmetrical thin carbon molecular sieving (CMS) membranes exhibiting good mechanical strength and high separation performance were prepared by changing the physical properties of α-Al_2O_3 substrates. The physical properties of the substrates, such as pore size, pore volume and surface roughness, significantly influence the penetrability of polymer solution and were systematically modified by sintering temperature, heating rate and dwell time. The tetradecahedral shape of the substrate achieved at the sintering temperature of 1400 °C was found to be suitable for the prepared CMS membranes, which exhibited a H_2 permeability of 1300 Barrer with H_2/CH_4 and CO_2/CH_4 selectivities of 174.16 and 56.44, respectively. To optimize the substrate structure to provide a cost-effective and highly productive method for the deposition of brittle CMS membranes, this proposed procedure can be used to improve the mechanical strength of the supported membrane for enhanced manipulation.

1. Introduction

Due to the demand for gas separation and purification technologies [1–6], inorganic membranes, such as zeolites [7–9], carbon molecular sieving (CMS) membranes [10–12], and metallic Pd membranes, have progressively grown in prominence. These materials have molecular sieve structures, which have applications in hydrogen purification, carbon capture and oxygen/nitrogen separations.

CMS membranes are fabricated using an amorphous carbon matrix that derived from polymer precursor. These membranes exhibit hydrophobicity and thermostability and are resistant to corrosion from planar molecules (e.g., ethylene, formaldehyde, and benzene). The pore structure of CMS membranes consists of micro and ultramicro pores, which can improve diffusibility and ensure high selectivity, respectively [11,13,14]. However, the primary disadvantage that impedes their commercialization is their brittleness, which requires careful handling [15].

CMS membranes can be divided into symmetric and asymmetric types according to their structure or shape. The symmetric types generally have insufficient mechanical strength to meet the various demands for high productivity and efficiency in industrial applications [16]. In comparison, the asymmetric-type membranes typically consist of a support layer, a top layer, and/or intermediate layers, which are beneficial for producing thin, selective carbon layers [17–19] and allow excellent separation performance and long term operation [20,21]. Haar and Verweij [22] proposed that the mechanical stability of the deposited layers strongly depends on the properties of the substrate and should meet the following requirements: (1) a narrow pore size distribution, (2) the ability to withstand the operation temperature, (3) similar thermal and chemical expansion properties as the top layer, (4) a permeation mechanism that is independent of the mass transport resistance, and (5) sufficient mechanical strength. At present, numerous researchers have used different substrates to prepare CMS membranes, such as stainless steel, carbon substrate, and ceramic substrate. However, the effect of substrate properties on the mechanical stability and separation performance of CMS membranes have not been sufficiently discussed.

Several researchers are making efforts to estimate the influences of substrate properties, such as surface roughness and pore size distribution, on the polymer and metallic membrane fields. Hamad et al. [20] used porous polyethersulfone (PES) as a substrate to prepare polyphenylene oxide (PPO)/PES asymmetric polymer membranes. The greater surface roughness of the substrate caused the bottom of the selective layer to be closely conglutinated with the substrate, thereby improving the selectivity of the selective layer. Wei at al. [23] coated a polymeric membrane onto a ceramic substrate to overcome the expansion

* Corresponding author at: Department of Occupational Medicine, Chung Shan Medical University Hospital, No.110, Sec. 1, Jianguo N. Road, Taichung City, Taiwan, ROC. Tel.: +886 4 2473 0022; fax: +886 4 2324 8194.
E-mail address: hhtseng@csmu.edu.tw (H.-H. Tseng).

0376-7388/$ - see front matter © 2013 Elsevier B.V. All rights reserved.
http://dx.doi.org/10.1016/j.memsci.2013.11.039

phenomena. The expansion was limited using a cross-linking process, which strengthened the adhesion between the separation layer and the ceramic substrate, especially when the surface roughness of the ceramic substrate is greater. Huber et al. [24] explored the O_2/N_2 separation performance by polymer plasma deposition onto the alumina substrate. These researchers studied the effect of pore size distribution in the substrate and found that evenly distributed pore sizes led to enhanced carriers. Moreover, the even distribution of pore sizes enabled the membrane to completely cover the pores of the substrate during deposition. In combination with the above-mentioned results, the pore size distribution of the substrate is conducive to the formation of a thin, continuous and defect-free selective layer.

To strengthen the mechanical stability of CMS membranes, porous materials, such as alumina, are typically used as a substrate for membrane fabrication. According to previous work in our lab, when an alumina substrate with relatively large pore sizes was used, the polymer precursor easily penetrated into the substrate. Dense and defect-free carbon membranes were not easily obtained, as this process required several coatings to form a defect-free top layer. However, when an alumina substrate with relatively small pore sizes was used, the polymer precursors could not easily penetrate into the substrate, and the marginal adaptability between the top layer and the substrate was reduced, resulting in a decrease of the membrane selectivity. Therefore, when using alumina as the carbon substrate, an appropriate pore size distribution is essential to the construction of the asymmetric carbon membrane, allowing high permeability and selectivity to be obtained through a simple preparation process. Lin et al. [25] have studied and compared the effects of α- and γ-Al_2O_3 support on the separation performances of CMS membranes. The Al_2O_3 support possessing a smaller pore size and smoother surface might be helpful for forming a thinner and better quality of the membrane, due to the reduce of thermal expansion mismatch between the carbonizing layer and the alumina support during pyrolysis. However, the effect of pore size distribution of Al_2O_3 supports on the separation performance was not evaluated.

The pore structure of the alumina is mainly controlled by sintering conditions, such as sintering temperature, heating rate, and soaking time, which affects the particle arrangement and pore size distribution. Wang et al. [26] have evaluated the effect of sintering conditions on particle arrangement and pore size distribution of micro-sized alumina. The results indicated that after the sintering treatment, the alumina particles were coarser, and the pores became larger during the early stage. As the temperature increased to 1400 °C, the alumina particles were transformed to a vermicular shape (also known as a tetradecahedral shape). This structure was relatively loose, and the total pore volume was increased. When the temperature rose to 1500 °C, the alumina particles gradually became denser, resulting in a significant reduction in the total pore volume. The pore structure completely collapsed above 1600 °C.

To optimize the substrate structure, we modified the porous structure and surface roughness of the α-Al_2O_3 substrate by controlling the sintering conditions, including sintering temperature, heating rate, and soaking time. To prevent the gas transport resistance within the alumina substrate from increasing due to sintering at high temperatures, the sintering temperature was maintained below 1600 °C.

2. Experimental

2.1. Pretreatment of α-Al_2O_3 substrates

The green disk-shaped nanoceramic α-Al_2O_3 substrates with approximately 23-mm diameter and 1.4-mm thickness were purchased from Ganya Fine Ceramics Co., Taiwan. These green substrates were prepared by compressing α-Al_2O_3 powder (purity > 99.5, Japan) with particle sizes ranging from 0.1 to 2 μm. The surface morphology and X-ray diffraction pattern are shown in Fig. 1. These substrates were sintered in air in the 1100–1400 °C temperature range with a dwelling time of 2–3 h and a ramping rate of 1–10 °C/min. The sintered substrates are hereafter referred to as substrate SX–Y–Z, where X, Y, and Z are the sintering temperature, ramping rate, and dwelling time, respectively. In the course of the experiment, the substrate sintering temperature was kept below 1500 °C to prevent an increased substrate resistance to mass transfer, a result of the sintering process which results in an increased density that impacts the overall mass transfer behavior of the membrane.

2.2. Preparation of CMS membrane

The asymmetric CMS membrane was prepared by a spin-coating method previously described [27]. A 10% polyetherimide (PEI) solution was spin-coated at 1000 rpm for 20 s on a substrate surface. The coated supporting polymer film was left overnight at ambient temperature for solvent evaporation, which was followed by curing in a vacuum oven at 240 °C for 6 h at a heating rate of 5 °C/min. The film was subsequently heated to 600 °C at a rate of 5 °C/min and held at that temperature for 2 h. Subsequently, the membranes were slowly cooled to room temperature and were stored in a desiccator containing silica gel. Prior to aging decay, within 24 h, the membranes were subjected to a gas permeance test. Hereafter, the resultant CMS membranes are renamed by replacing the "S" in the original name of the corresponding substrate with an "M". For example, the carbon membrane fabricated with an S1100-1-2 substrate is designated as M1100-1-2.

2.3. Characterization of substrates and CMS membranes

The porous structures were measured using N_2 sorption at −196 °C with a PMI automated Brunauer–Emmett–Teller (BET) sorptometer (201AEL). The crystalline structure were recorded by X-ray diffraction (XRD) using a PW1830 X-ray powder diffractometer (Philips) with a Cu-K_α source ($\lambda = 1.5418$ Å) in a wide Bragg angle range ($20^\circ \le 2\theta \le 70^\circ$) with a 2°/min scanning rate. The surface roughness was measured by atomic force microscopy in the non-contact mode using a C26 Dualscope/Rasterscope scanner (DME, Denmark). The surface morphology and cross-sectional images were examined by field-emission scanning electron microscopy (FE-SEM; JSM 5600). The mechanical strength was measured by biaxial pressure mode.

2.4. Gas permeation test

The gas permeance experiments were performed using the steady-state gases H_2, CO_2, O_2, N_2, and CH_4 at room temperature (25 ± 2 °C). The permeate side of the membrane was degassed in a vacuum before testing, whereas a pressure of 2 atm was applied on the feed side. The gas permeance was calculated from the slope (dP/dt) of the plot of pressure (P) versus time (t) using the following equation:

$$\text{Permeability}, Q = \left(\frac{dP}{dt}\right) \times \frac{VT_0}{A\Delta P} \times \frac{L}{TP_0} \quad (1)$$

where dP/dt is the rate of pressure increase at steady state, V is the downstream gas permeation volume (in cm^3), A is the membrane area (in cm^2), ΔP is the differential pressure across the membrane, L is the membrane thickness (in cm), P_0 is 76 cm Hg, T_0 is 273 K, and T is the measured temperature (in K).

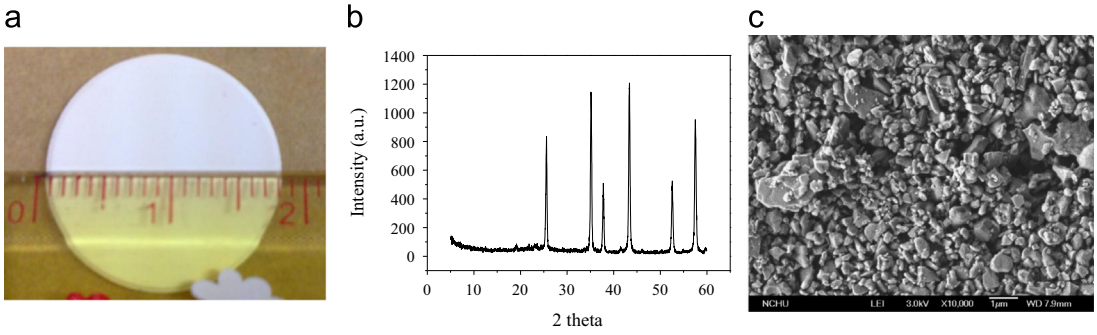

Fig. 1. (a) Surface morphology, (b) X-ray diffraction pattern, and (c) FE-SEM images of green disk-shaped α-Al_2O_3 supports. (For interpretation of the references to color in this figure legend, the reader is referred to the web version of this article.)

The ideal selectivity coefficient of pure gas A/B ($\alpha_{A/B}$) is defined as the ratio of the permeability of A to that of B:

$$\alpha_{A/B} = \frac{Q_A}{Q_B} \quad (2)$$

The average values and standard deviation were determined from six samples of two batches.

3. Results and discussion

3.1. Effect of the sintering conditions on the chemical-physical properties of the substrates

3.1.1. Crystal phase

The influence of the different sintering parameters on the crystal phase and crystal size of the alumina substrate is shown in Fig. 2 and Table 1. The crystal size, calculated by the diffraction patterns (use different sintering temperatures as examples) and Schere's formula, indicated that there was no significant change in the crystal phase and size of the alumina. Each substrate had a crystal size range of 34.1–38.0 nm and exhibited no change between different sintering conditions because the α-Al_2O_3 powder used for the spindles had already been subjected to a high temperature sintering process at 1600 °C. This temperature was higher than the sintering temperatures used in this study. Therefore, the crystal phase and size did not change significantly under different sintering conditions.

3.1.2. Pore structure

Table 1 shows the influence of the different sintering parameters on the specific surface area, average pore radius and pore volume of the substrates. It was found that as the sintering temperature increased from 1100 °C to 1400 °C, the specific surface area of the α-Al_2O_3 substrates decreased from 5.9 to 1.6 m^2/g. The average pore size increased from 78.63 to 107.40 Å. The pore volume decreased from 0.0116 to 0.0043 cm^3/g. The overall pore structure indicated an apparent loss as the sintering temperature increased. As shown in Fig. 3(a), the difference of pore volume was most significant for pore sizes between 15 and 40 Å. These observations indicate that the high sintering temperature results in a higher diffusion coefficient and thus accelerates the sintering of alumina substrates [27]. Based on the sintering theory model proposed by Ashby [28], the curvature around the neck of the alumina particles during the early stage of sintering and the high temperatures enabled the particles to diffuse. As a result, the contact surface between the alumina particles was slowly transformed into a neck shape during the early stage of sintering. At this stage, the pore shrank but remained in the open state. The same tendency is observed from past research [28]. As the

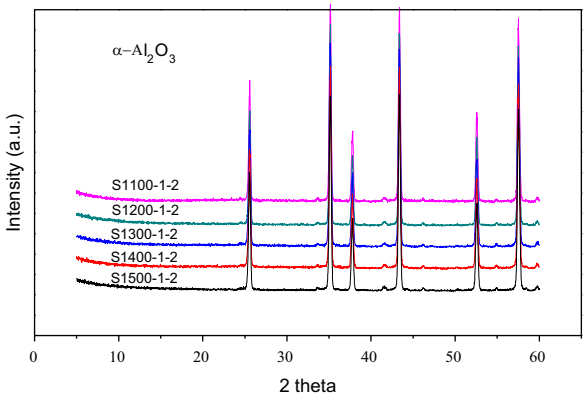

Fig. 2. X-ray diffraction pattern of α-Al_2O_3 supports sintered at different temperatures.

sintering temperature continued to rise to 1500 °C, all sintering diffusion mechanisms continued to occur. During this stage, interparticle pores developed on the edges and corners of the grains, making the movement of the grain boundary unfavorable. Therefore, at this stage, the grain growth was less obvious. The pore structure slowly disintegrated and gradually became smooth in shape. In addition, the grain was transformed into a 14-sided columnar body. The particles were fast-growing and tended to be dense (as shown in Table 1, the pore structure could not be measured by an analyzer). This phenomenon can be clearly observed in the FE-SEM images in Fig. 4, which demonstrate that the alumina particles diffused into larger particles. The contact surface of the particles increased significantly, resulting in decreases of the specific surface area and the overall pore volume.

The influence of the sintering heating rate on the pore structure of alumina was also significant. As shown in Table 1 and Fig. 3(b), when the heating rate was reduced from 10 °C/min to 1 °C/min, the specific surface area was clearly observed to decrease. In addition, the average pore diameter increased, and the pore volume decreased. This trend is also observed when the sintering temperature is increased. This phenomenon could be explained in that the slow heating rate helped the alumina particle transform into a tetradecahedral shape, resulting in the apparent loss of the pore structure. This result was consistent with the FE-SEM image. Fig. 4(d) and (f)–(h) shows that the particle size increased when the heating rate was decreased.

The influence of the dwell time on the pore structure and pore size distribution of the alumina substrate is shown in Table 1 and Fig. 3(c). When the dwell time increased from 2 to 3 h, there was no significant difference in the specific surface area, pore volume and pore diameter distribution. It is possible that the selected

Table 1
Effect of sintering conditions on chemical-physical properties of α-Al_2O_3 supports.

Code	Crystal size (nm)	S_{BET} (m^2/g)	D_{pore} (Å)	V_{total} (cm^3/g)	BJH adsorption cumulative pore volume of pores between 13.5 and 1000 Å (cm^3/g)		
					V_{micro}	V_{meso}	V_{macro}
S1100-1-2	34.1	5.9	78.63	0.0116	0.0021	0.0082	0.0011
S1200-1-2	35.9	4.3	76.54	0.0084	0.0017	0.0058	0.0008
S1300-1-2	35.9	3.1	80.16	0.0061	0.0011	0.0044	0.0005
S1400-1-2	37.5	1.6	107.40	0.0043	0.0005	0.0033	0.0003
S1500-1-2	38.0	N.D.	N.D.	N.D.	N.D.	N.D.	N.D.
S1400-2-2	36.8	4.3	74.22	0.0080	0.0011	0.0063	0.0005
S1400-5-2	36.3	5.2	66.48	0.0087	0.0012	0.0062	0.0005
S1400-10-2	36.5	5.2	66.00	0.0086	0.0012	0.0068	0.0005
S1400-2-3	36.0	4.3	74.10	0.0080	0.0011	0.0062	0.0005

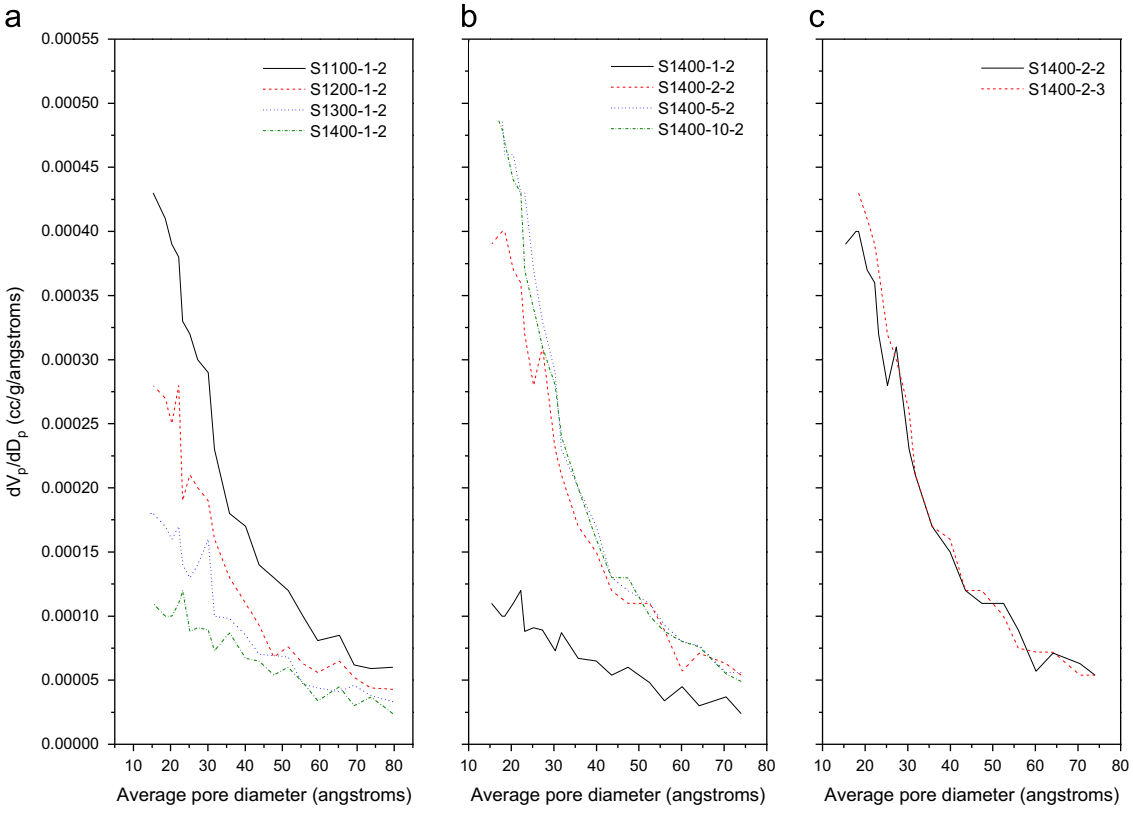

Fig. 3. Effects of (a) sintering temperature, (b) heating rate, and (c) dwell time on the pore size distribution of α-Al_2O_3 substrates.

dwell times were sufficiently similar for the influence of the dwell time on the pore structure not to be observable.

3.1.3. True density and volume shrinkage

Fig. 5 shows the substrate volume shrinkage of as a function of sintering temperature. It was observed that the substrate volume shrinkage increased as the sintering temperature increased from 0.55% (1100 °C) to 16.55% (1500 °C). Under the different sintering temperatures, the volume shrinkage rate can be divided into two stages: (1) first, as the temperature increased from 1100 to 1400 °C, higher shrinkage rate was exhibited due to particle coarsening; (2) second, as the temperature increased from 1400 to 1500 °C, a lower shrinkage rate was observed due to the green body densification.

3.1.4. Surface roughness

Fig. 6 shows the AFM images of the alumina substrates treated under different sintering conditions. When the sintering temperature of the substrate increased from 1100 to 1500 °C, the surface roughness coefficient (Ra) of the substrate increased from 38.8 to 103.0 nm. The increased surface roughness could be a result of alumina particle coarsening and densification, causing the surface roughness coefficient to increase as the sintering temperature increased.

With the sintering temperature fixed at 1400 °C and the heating rate reduced from 10 to 2 °C/min, the surface roughness coefficient of the substrate decreased from 67.6 to 42.8 nm. The slow heating rate provided the alumina particles with enough heat energy to transform into a tetradecahedral structure. Therefore, the substrate surface became relatively homogeneous when the heating rate was decreased. However, when the heating rate was further decreased to 1 °C/min, the surface roughness coefficient increased from 42.8 to 69.7 nm because the relative surface roughness became heterogeneous when the alumina density increased. Table 2 summarizes similar results obtained from different dwell time conditions. When the sintering temperature and heating rate were fixed at 1400 °C and 2 °C/min, respectively,

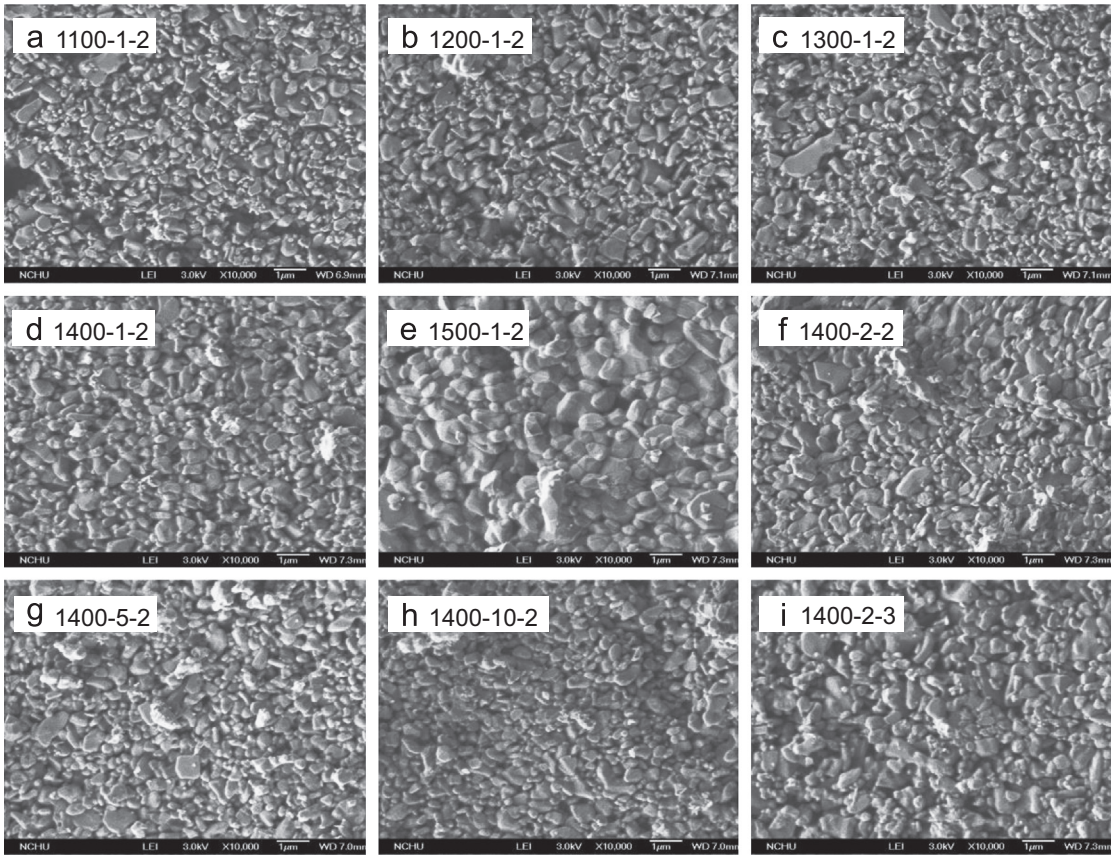

Fig. 4. FE-SEM images of α-Al_2O_3 substrates treated under different sintering conditions.

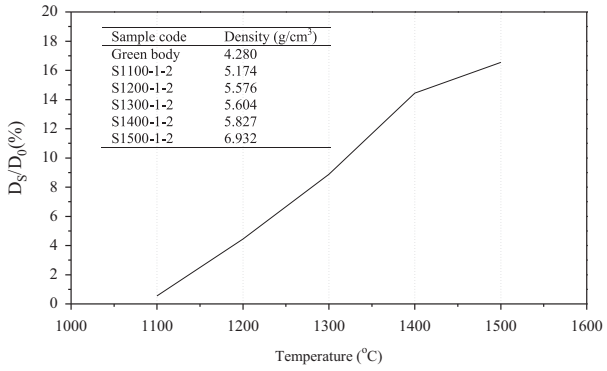

Fig. 5. Volume shrinkage of substrates as a function of sintering temperature.

the surface roughness coefficient increased from 53.1 to 75.5 nm when the dwell time increased from 2 to 3 h. A relatively extended dwell time increased the degree of coarsening for the alumina particles, making the surface of the substrate relatively heterogeneous and thereby enhancing the surface roughness coefficient.

The XRD, BET, FE-SEM and AFM results are integrated in a schematic diagram in Fig. 7 to exhibit the change in the alumina substrate structure with respect to sintering temperature. The particle sintering behavior can be divided into three heating stages: (1) from ambient to 1300 °C, the alumina particles coarsened and were subsequently restacked, leading to a reduced pore volume and increased surface roughness. (2) When the temperature was elevated to 1400 °C, the alumina particles started to change to the tetradecahedral shape and increased in density. Consequently, the pore volume decreased. The surface roughness continued to increase due to tetradecahedral particle aggregation. (3) When the temperature rose to 1500 °C, the alumina particles became very dense, resulting in a notably low substrate pore volume. The surface roughness was also relatively heterogeneous. Therefore, a series of phenomena associated with the increased sintering temperature (including particle growth, coarsening and densification) was the main reason for the increase in the surface roughness and decrease in the pore volume.

3.2. *The characterization of the α-Al_2O_3 supported CMS membrane*

3.2.1. *The morphology and d-spacing of the carbon matrix*

The FE-SEM microphotographs of CMS membranes supported on different α-Al_2O_3 substrates are shown in Fig. 8. It can be observed that these surface images show a smooth, almost defect-free morphology (Fig. 8(a1)–(i1)). Carbon layers with dense matrix structures were sequentially deposited on the α-Al_2O_3 substrates, even under different sintering conditions. Furthermore, good adherence between the top layer and the alumina substrate was observed. The thickness of the PEI-derived carbon layers approximately measured 2.9–5.6 μm (as shown in Table 3). The highest thickness (5.550 μm) of the CMS layer was obtained from the M1500-1-2 membrane.

The d-spacing of carbon membranes refers to the interlayer distance of the carbon matrix and can also be considered to be the pore size relevant for the transport of gas molecules through the carbon membranes. As indicated in Table 2, the change in the d-spacing of the carbon membranes showed a bimodal trend when the sintering temperature of the substrate was increased from 1100 °C to 1500 °C. The d-spacing values of M1200-1-2 and M1400-1-2 were larger than that of other membranes. This phenomenon was significantly different than other trends: with increasing sintering temperature, reduced specific surface area

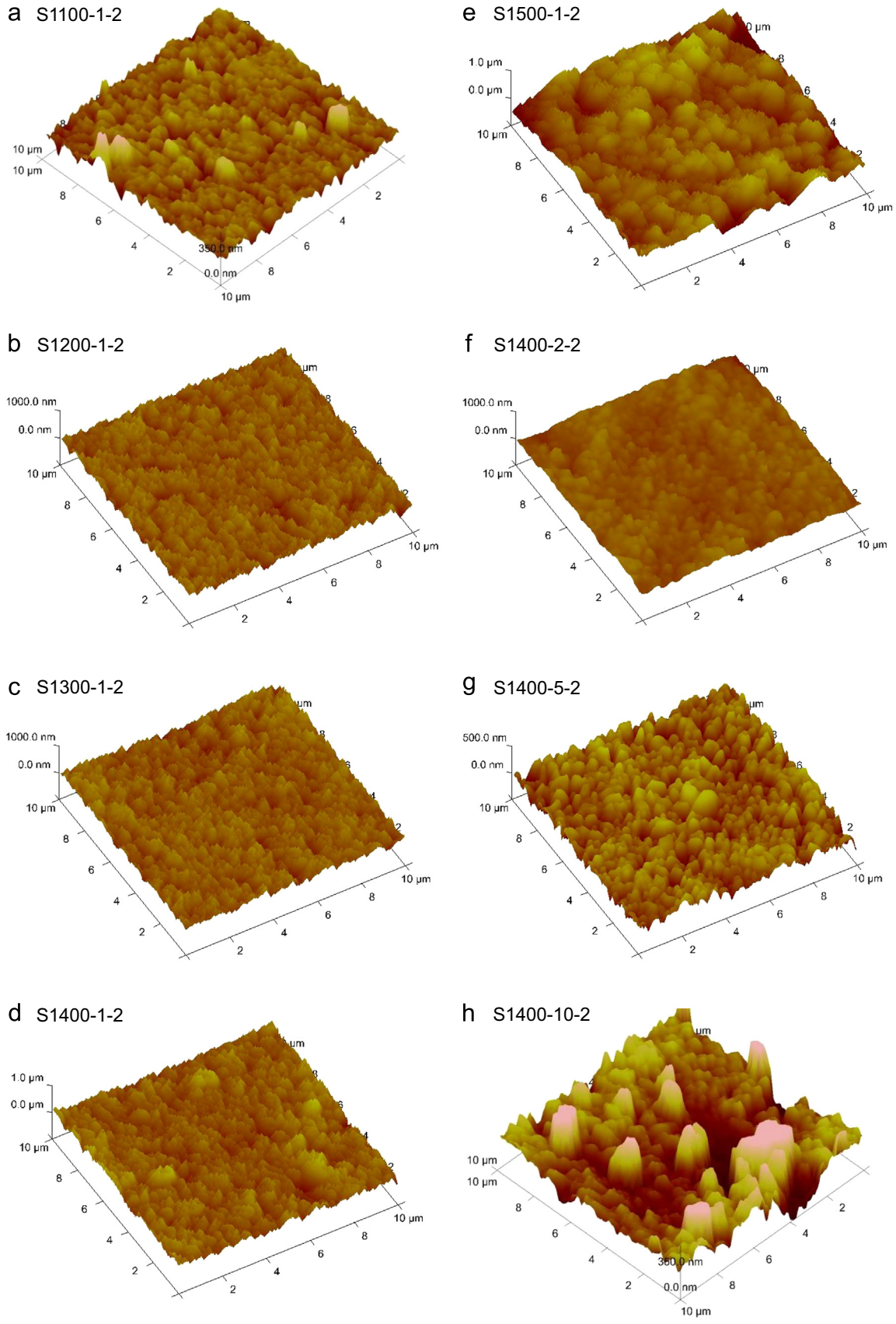

Fig. 6. AFM images of α-Al_2O_3 substrates treated under different sintering conditions.

and total pore volume or increased average pore size and surface roughness were observed, as described above for the alumina substrate. Note that this finding cannot be explained by random occurrence because the permeability through these membranes are strongly correlated with the d-spacing value (see Section 3.3). Several effects could be responsible for the observed bimodal-type

d-spacing value. Because d-spacing value is the distance between the stacked carbon matrix layers, it directly affects by the physical properties of the alumina substrate. Therefore, it can be inferred that the trends observed in the d-spacing values are caused by the combined effects of both pore structure and surface roughness of α-Al_2O_3 substrates. Theoretically, the interlayer distance of the carbon matrix was formed from the gap generated after pyrolysis when the aromatic compounds were irregularly stacked on the polymer precursor-coated substrate, thereby determining by the pore structure and the surface roughness of the substrate. Generally speaking, when the pore sizes of the substrate are larger, the casting dope more readily penetrates into the pores of the substrate during the coating process. The casting dope is deposited not only on the surface but also within the pores, resulting in a strong mechanical interlock (see. Section 3.2.2.) with the substrate, which leads to larger d-spacing values. In contrast, with smaller pores, casting dope less readily penetrates into the substrate, resulting in a relatively thick membrane and relatively smaller d-spacing values (e.g., M1500-1-2). The surface roughness also exerts significant influence on the d-spacing values. When the substrate surface is rougher, the folding of the polymer chains is more irregular and prominent, resulting in a larger interlayer distance after carbonization. Therefore, it is expected that the d-spacing values exhibit a bimodal trend due to the combined effects of the reduced substrate pore structure and the increased surface roughness.

The above assumptions can be verified by the results obtained from the substrates treated with different dwell times and heating rates. As indicated in Table 2, the surface roughness of the alumina substrate can be increased by controlling the dwell time while maintaining a constant pore structure. The d-spacing also increases with increasing roughness when the pore structure remains unchanged. For heating rates in the range of 2–10 °C/min, the pore structure, surface roughness and d-spacing all decrease when the heating rate is reduced. Therefore, a decrease in the pore structure also decreases the d-spacing.

3.2.2. *Mechanical strength*

Fig. 9 shows the mechanical strength measured by the bi-axial method. The average strength of 185 N is high enough when compared with that of conventional alumina ceramics. It was

Table 2
d-Spacing, surface roughness, and membrane thickness of CMS membranes supported on various α-Al_2O_3 supports.

Sample code	Membrane thickness (μm)	d-Spacing (Å)	Ra of support (nm)	Ra of membranes (nm)
M1100-1-2	4.237	4.47	38.8	55.3
M1200-1-2	4.219	4.51	57.2	73.6
M1300-1-2	3.722	4.32	60.4	48.3
M1400-1-2	4.144	4.64	69.7	64.2
M1500-1-2	5.550	4.02	103.0	123.0
M1400-2-2	4.800	4.32	42.8	44.4
M1400-5-2	4.500	4.62	61.0	92.0
M1400-10-2	4.313	4.76	67.6	107.0
M1400-2-3	2.981	4.64	59.4	52.9

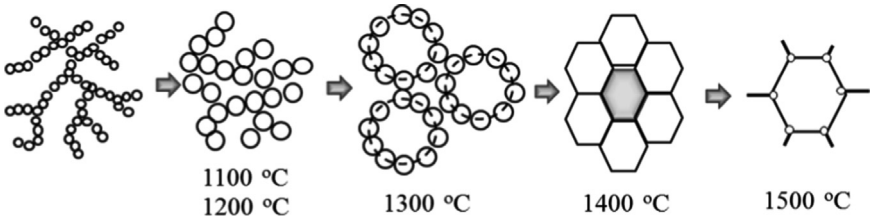

Fig. 7. Schematic of the changing in the alumina substrate structure with respect to sintering temperature (adapted from ref [27]).

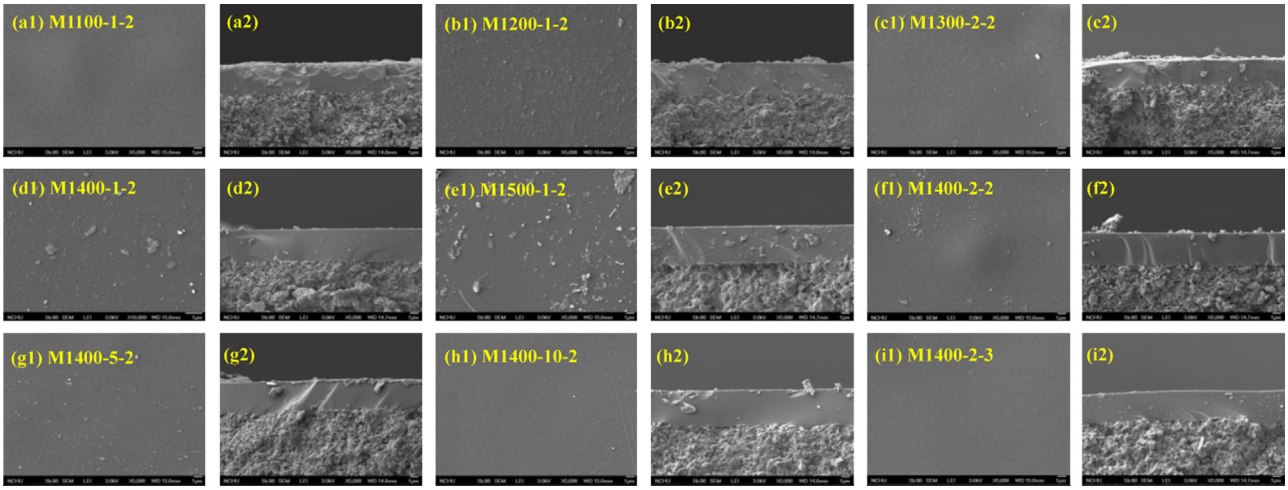

Fig. 8. FE-SEM images of (1) surface view and (2) cross-sectional view of CMS membranes supported on various γ-Al_2O_3 substrates.

found that the strength of M1400-2-3 was higher than the other three membranes. This could be explained by average pore size, that it is resulted from the effect of sintering pretreatment, i.e., a suitable sintering treatment is required in the improving the mechanical strength of α-Al_2O_3 supported CMS membranes.

3.3. Gas separation performance

Fig. 10 and Table 3 present the effects of substrate properties on the performance of the CMS membranes based on the pure gas permeation rate and permselectivity for the gas pairs of H_2/CH_4, CO_2/CH_4, and O_2/N_2 against (a) sintering temperature, (b) heating rate, and (c) dwell time, respectively. As shown in Fig. 10, it can be observed that the gas permeability increased with the gas kinetic diameter in the following order: $H_2 > CO_2 > O_2 > N_2 > CH_4$. This observation is consistent with the mechanisms of molecular sieving.

The effect of the substrate sintering temperature on the gas permeability is shown in Fig. 10(a). Based on the estimated membrane thicknesses given in Table 2, the hydrogen permeabilities at 25 °C are 2112.2, 2304.38, 385.71, 1532.34, and 102.67 Barrer for membranes M1100-1-2, M1200-1-2, M1300-1-2, M1400-1-2, and M1500-1-2, respectively. It seems that the trend in the gas permeability was consistent correlated with the d-spacing value, where the gas permeability increased as the d-spacing increased, and the gas permeability decreased as the d-spacing decreased. Previously study also indicated that a similar trend was observed when the d-spacing value was changed [29]. The gas diffusion path increased with increasing d-spacing, which results in high permeability. The effects of the sintering heating rate and dwell time of the substrate on the gas permeability are shown in Fig. 10(b) and (c). These figures also show that the gas permeability increased as the d-spacing increased.

The gas pair selectivities of CMS membranes supported on substrates treated with different sintering temperatures are indicated in Table 3. Comparison of the selectivity of CMS membrane with sintering temperature indicates increases as high as 11.3 times in the H_2/CH_4 separation factor for the membrane supported on the S1400-1-2 substrate compared to that on the S1100-1-2 substrate. The observed increases in permselectivity are significantly larger than those expected from other sintering temperatures; similar results were also observed for the gas pairs CO_2/CH_4 (20.6 times) and O_2/N_2 (4.7 times). The sintering of α-Al_2O_3 substrates at the high temperature of 1400 °C appears to be a contributing factor to the increases in the selectivities of the CMS membranes.

The hypothetical path of a gas molecule permeating through the carbon film on the sintered substrate is depicted in Fig. 11. The route has three identifiable regions: the carbon film on the surface, the carbon matrix in contact with alumina (i.e., carbon matrix penetration into the substrate, see Fig. 12), and the pore of substrate. As mentioned above, the influence of sintering is expected to be primarily centered around the carbon matrix in the first two regions. The resistance model is utilized to assess the effect of the penetration of the carbon matrix into the pores of the

Table 3
Gas pair selectivity of CMS membranes supported on α-Al_2O_3 substrates treated with different sintering conditions.

Sample code	Selectivity		
	H_2/CH_4	O_2/N_2	CO_2/CH_4
M1100-1-2	5.94 ± 1.27	1.15 ± 0.16	1.51 ± 0.48
M1200-1-2	5.06 ± 1.76	1 ± 0.04	1.4 ± 0.38
M1300-1-2	17.05 ± 3.44	2.38 ± 0.55	5.21 ± 0.65
M1400-1-2	67.31 ± 4.61	5.41 ± 0.46	31.08 ± 10.05
M1500-1-2	9.05 ± 6.20	1.51 ± 1.12	1.86 ± 1.40
M1400-2-2	174.16 ± 39.05	8.05 ± 0.81	56.44 ± 8.9
M1400-5-2	89.32 ± 6.41	6.73 ± 1.43	28.63 ± 3.64
M1400-10-2	57.66 ± 18.20	5.12 ± 0.96	18.39 ± 2.79
M1400-2-3	76.35 ± 14.21	5.73 ± 0.50	25.44 ± 3.66

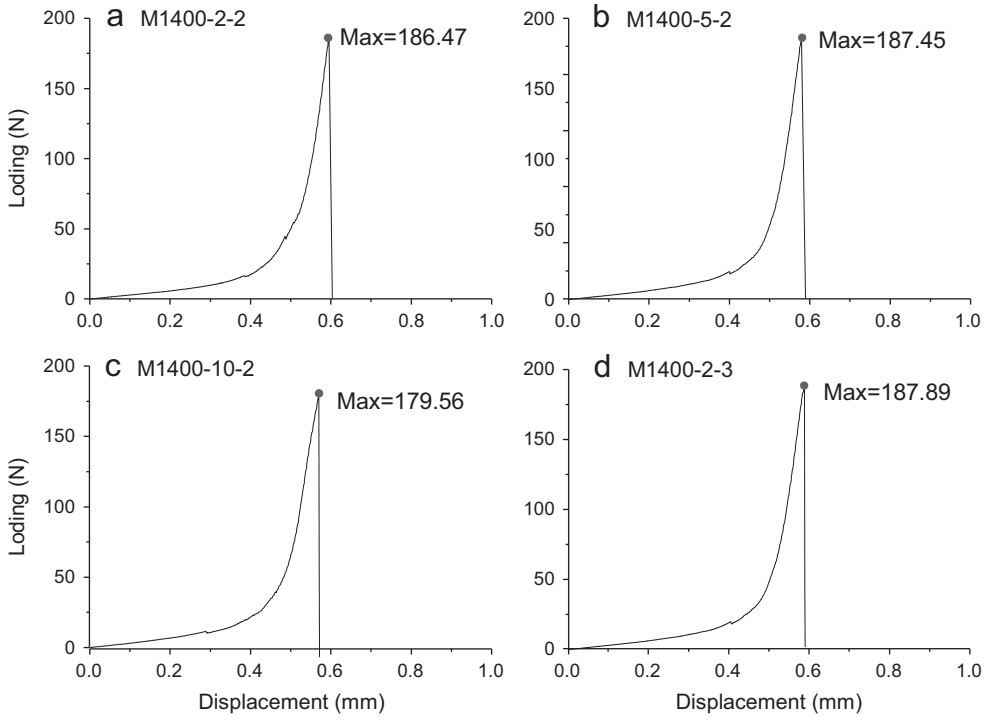

Fig. 9. Mechanical strength of CMS membrane supported on various supports.

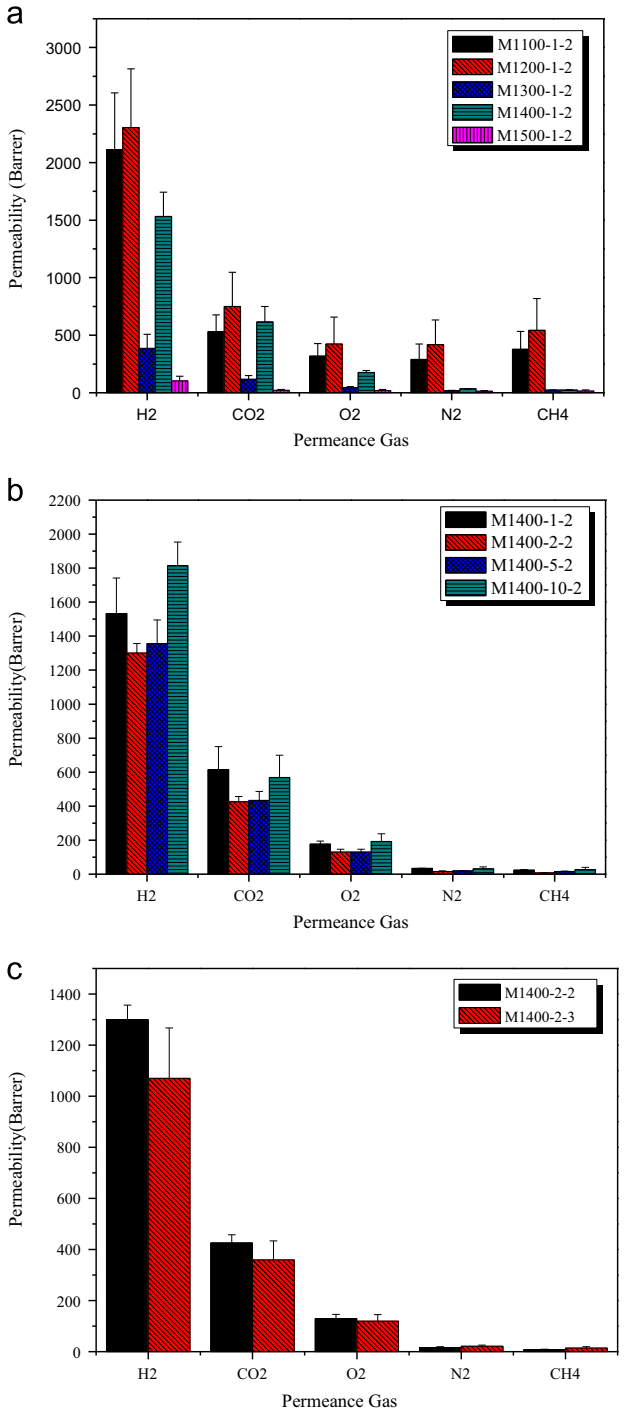

Fig. 10. Gas permeability of CMS membranes supported on α-Al_2O_3 substrates treated with different (a) sintering temperatures, (b) heating rates, and (c) dwell times.

different substrates on the overall performance of the supported membranes [20,30]. The overall resistances of the supported CMS membranes are defined by the following equations:

$$R_T = R_1 + R_2 + R_3 \tag{3}$$

$$\frac{\ell_T}{P_T} = \frac{\ell_1}{P_1} + \frac{\ell_2}{P_2} + \frac{\ell_3}{P_3} \tag{4}$$

where ℓ is the thickness of carbon layers, P is the permeability, and the suffixes 1, 2, and 3 of ℓ and P are the permeance routes. The resistance of the substrate, ℓ_3/P_3, is assumed to be negligible because the treated substrate still retains a fairly high flux P_3 value, indicating insignificant resistance to gas flow (no observable significant difference was recorded for the gas flux prior to and after sintering). Therefore, the overall resistance of the supported CMS membrane is integrated with the resistance of the carbon film on the surface and the resistance of the carbon film penetration into the substrate. Therefore, based on Eq. (4), a reduction of the thickness of the surface film should further increase the overall selectivity of the supported membrane. This effect was verified by Moaddeb and Koros [30]. They systematically reduced the thickness of the polymer membrane by changing the concentration of the casting dope. As the amount of the deposited polymer was reduced, the separation factor of the membrane increased. However, for the supported membrane, the actual effective thickness, $\ell_1+\ell_2$, is not precisely known due to the penetration of carbon matrix into the pores of the substrate. The sintering of the α-Al_2O_3 substrates increased the average pore size but also reduced the pore volume inside the pores; therefore, even a small amount of polymer could enter the substrate pores. Table 2 presents the "apparent thickness" of film on the surface, as measured from the FE-SEM images of the cross sections of the supported membranes. The results indicated that the apparent thickness was decreased when the sintering temperature increased to 1300 °C, and subsequently increased by 1500 °C. In contrast with the pore size and pore volume illustrated in Table 1, the larger pore size was helpful for polymer penetration into the pores, but the penetrating amount of polymer was restricted by the total pore volume, Therefore, the smallest thickness was obtained from M1300-1-2 due to its larger pore size but not the smallest pore volume. The penetrated carbon matrix is in contact with α-Al_2O_3 particles to increase mechanical interlocking, which has a higher permselectivity than the surface carbon membrane. So a reduced surface film thickness will increase the contribution from the more selective composite layer. It was for this reason that the selectivity of the membranes initially increased with sintering temperature followed by a decrease in value.

For practical application, an increase in selectivity accompanied by an unapparent loss in permeability is expected. However, the M1400-1-2 membrane exhibits the highest selectivity, but a loss in permeability was still observed. Even considering these values of gas permeability, the separation performances of the CMS membrane supported on S1400-1-2 substrates are improved by raising

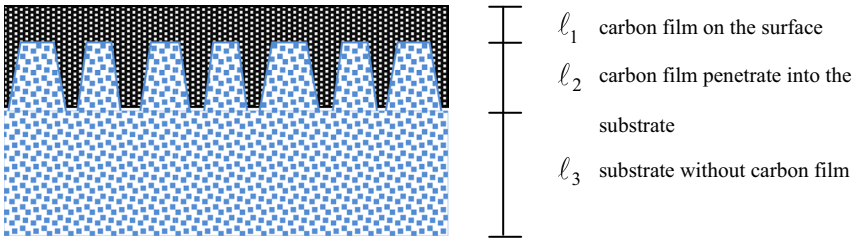

Fig. 11. The hypothetic path of a gas molecule permeating through the carbon film on the sintered substrate.

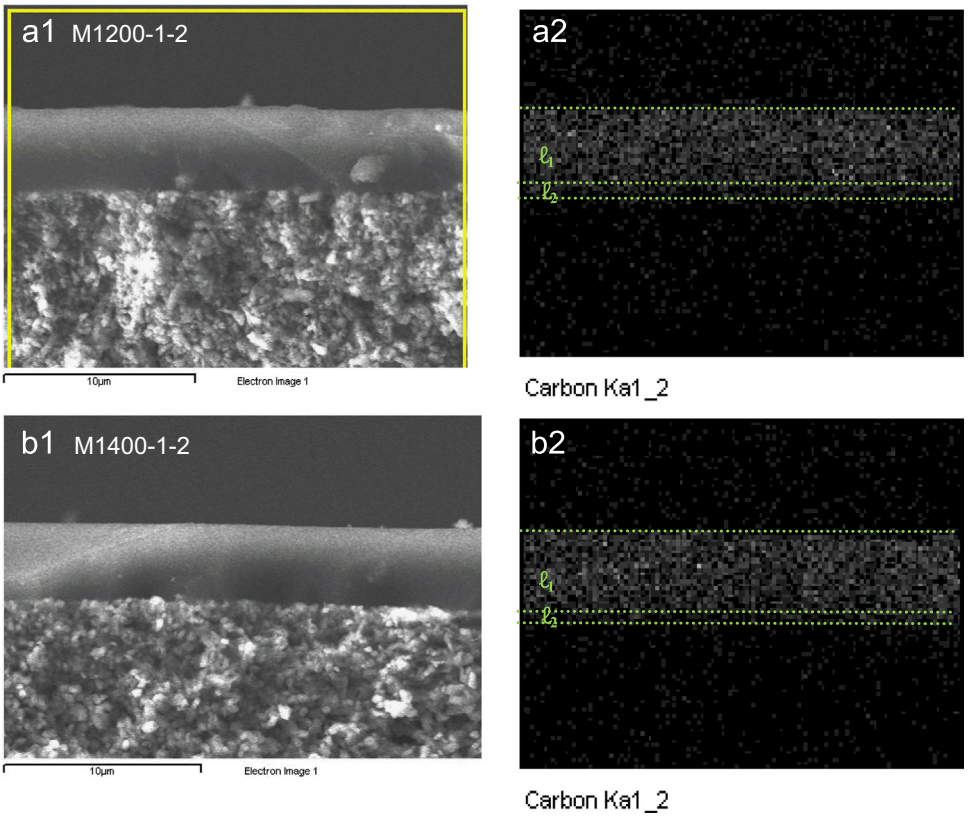

Fig. 12. (1) FE SEM photographs and (2) EDS maps of (matrix distributions in CMS composit membranes: (a) MI200-2 and (b) MI400-1-2.

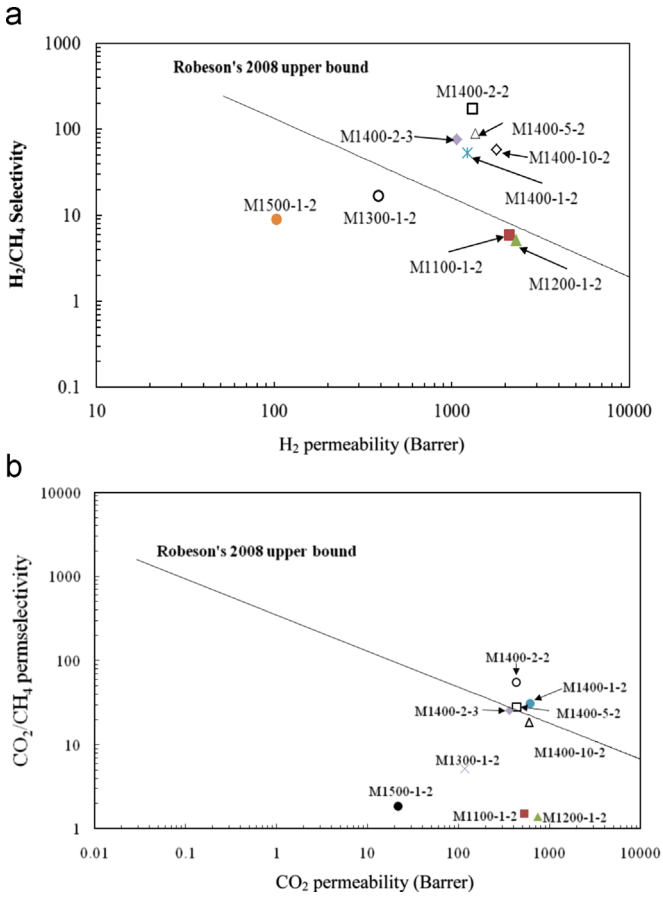

Fig. 13. Gas separation performance of CMS membrane compared with Robeson's 2008 upper bound: (a) H_2/CH_4 and (b) CO_2/CH_4.

the sintering temperature surpassing the 2008 Robeson's line [31] (as shown in Fig. 13).

Fig. 10(b) and (c), and Table 3 show the effects of heating rate and dwell time of α-Al_2O_3 substrates on gas permeability and selectivity. As shown in Fig. 10(b), the H_2 permeability gradually decreased from 1796.89 to 1300.3 Barrer, while the selectivity of H_2/CH_4 increased from 57.66 to 174.16 with a decreasing heating rate of 10–2 °C/min, due to the stacked, increased packing density of the carbon matrix (i.e., low d-spacing values) and the thick carbon film. Similar results were also observed in other gases and gas pair separation performances. Additionally, these observations also surpassed the 2008 Robeson's line [31] (as shown in Fig. 13).

Using the upper-bound relationship proposed by Robeson (2008) [31], this study selected membranes with high gas permeability and high selectivity. The comparison results are shown in Fig. 13. Among the membranes prepared using different sintering conditions, it was found that the carbon membranes supported by carrier bodies at sintering temperatures of 1400 °C showed the best permeability and selectivity performance for H_2/CH_4 and surpassed the upper-bound line. Similarly, only the M1400-1-2, M1400-2-2 and M1400-5-2 membranes were found to surpass the upper-bound line of CO_2/CH_4. Based on the above results, this study found that the M1400-2-2 membrane exhibited a high permeability and selectivity performance. Moreover, this membrane surpassed the upper-bound lines for the H_2/CH_4 and CO_2/CH_4 gas pairs proposed by Robeson (2008) [31], which was suitable for H_2 purification and CO_2 capture.

The perm-selectivities of selected CMS membranes derived from PEI precursor are summarized and compared with the present work in Table 4. The H_2 and/or CO_2 separation performances of the present membranes are impressive compared with other membranes reported in the literature, indicating the advantage of optimizing the substrate structure by altering sintering conditions. Optimization can simplify the coating-pyrolysis cycles into a single cycle to avoid a complex and high-energy demanding

Table 4
The perm-selectivities of CMS membranes from the literature compared with the present work.

Precursor/support	Preparation conditions	$P(H_2)$ (Barrer)	$P(CO_2)$ (Barrer)	H_2/CH_4	CO_2/CH_4	Reference
PEI/carbon	–	–	38	–	31.0	[32]
PEI/α-Al_2O_3	Post-treatment with self-assisted deposition carbon segment	811.6	512.5	136.3	86.1	[33]
PEI/α-Al_2O_3	Concentration of casting dope and pyrolysis temperature	198	50	46	11	[2]
PEI/α-Al_2O_3	Incorporation of SBA-15 mesoporous silica	667.5	222.5	75	25	[34]
PEI/α-Al_2O_3	Substrate structure	1200	458	84	33	[35]
PEI/α-Al_2O_3	Modified the support structure with sintering treatment	1300.3	426.1	174.2	56.4	This work

process and to improve the productivity of defect-free carbon membranes.

4. Conclusion

The optimum substrate structures for CMS membranes deposition were evaluated with various α-Al_2O_3 substrates. In this study, nanoceramics α-Al_2O_3, which has the pore size in the nanolevel was used as the supporting materials. As shown in the content and Table 1, the Dpore of the supports sintered at different temperatures are between 50 and 110 Å (5–11 nm), which is substantially smaller than the pore size of around 100–200 nm for the α-alumina supports used in other reported work. Due to the specific property of the alpha-alumina used in this work, the influence of support structure can be systematically studied. The physical properties, such as pore size distribution, total pore volume and surface roughness of α-Al_2O_3 substrates, were changed under different sintering conditions. As the sintering temperature increased, the pore structure of α-Al_2O_3 substrate was diminished, and the surface became rougher. When the sintering temperature reached 1500 °C, a densified pore structure was observed. The tetradecahedral shape of the substrate was achieved at the sintering temperature of 1400 °C, which was found to be suitable for the preparation of defect-free and high performance H_2- or CO_2-separation CMS membranes; additionally, decreasing the heating rate and dwell time were also benefit for increasing the permselectivity without significantly changed in permeability.

Acknowledgments

The authors would like to gratefully acknowledge the financial support provided by the NSC program (NSC 100-2221-E-040-004-MY3).

References

[1] G.Q. Lu, J.C. Diniz da Costa, M. Duke, S. Giessler, R. Socolow, R.H. Williams, T. Kreutz, Inorganic membranes for hydrogen production and purification: a critical review and perspective, J. Colloid Interface Sci. 314 (2007) 589–603.
[2] A.K. Itta, H.H. Tseng, Hydrogen separation performance of CMS membranes derived from the imide-functional group of two similar types of precursors, Int. J. Hydrog. Energy 36 (2011) 8645–8657.
[3] M. Bikshapathi, A. Sharma, N. Verma, Preparation of carbon molecular sieves from carbon micro and nanofibers for sequestration of CO_2, Chem. Eng. Res. Des. 89 (2011) 1737–1746.
[4] A. Brunetti, F. Scura, G. Barbieri, E. Drioli, Membrane technologies for CO_2 separation, J. Membr. Sci. 359 (2010) 115–125.
[5] C.W. Jones, W.J. Koros, Characterization of ultramicroporous carbon membranes with humidified feeds, Ind. Eng. Chem. Res. 34 (1995) 158–163.
[6] V.C. Geiszler, W.J. Koros, Effects of polyimide pyrolysis conditions on carbon molecular sieve membrane properties, Ind. Eng. Chem. Res. 35 (1996) 2999–3003.
[7] M.J. Muñoz-Aguado, M. Gregorkiewitz, Preparation of silica-based microporous inorganic gas separation membranes, J. Membr. Sci. 111 (1996) 7–18.
[8] X. Xu, Y. Bao, C. Song, W. Yang, J. Liu, L. Lin, Synthesis, characterization and single gas permeation properties of NaA zeolite membrane, J. Membr. Sci. 249 (2005) 51–64.
[9] J.C. Poshusta, R.D. Noble, J.L. Falconer, Temperature and pressure effects on CO_2 and CH_4 permeation through MFI zeolite membranes, J. Membr. Sci. 160 (1999) 115–125.
[10] P. Tin, T. Chung, Y. Liu, R. Wang, Separation of CO_2/CH_4 through carbon molecular sieve membranes derived from P84 polyimide, Carbon 42 (2004) 3123–3131.
[11] M. Kiyono, P.J. Williams, W.J. Koros, Effect of polymer precursors on carbon molecular sieve structure and separation performance properties, Carbon 48 (2010) 4432–4441.
[12] M.C. Campo, F.D. Magalhães, A. Mendes, Carbon molecular sieve membranes from cellophane paper, J. Membr. Sci. 350 (2010) 180–188.
[13] T. Kyotani, Control of pore structure in carbon, Carbon 38 (2000) 269–286.
[14] M. Kiyono, P.J. Williams, W.J. Koros, Effect of pyrolysis atmosphere on separation performance of carbon molecular sieve membranes, J. Membr. Sci. 359 (2010) 2–10.
[15] C. Song, T. Wang, H. Jiang, X. Wang, Y. Cao, J. Qin, Gas separation performance of C/CMS membranes derived from poly/furfuryl alcohol (PFA) with different chemical structure, J. Membr. Sci. 361 (2010) 22–27.
[16] A.F. Ismail, L.I.B. David, A review on the latest development of carbon membranes for gas separation, J. Membr. Sci. 193 (2001) 1–18.
[17] M.E. Rezac, W.J. Koros, Preparation of polymer–ceramic composite membranes with thin defect-free separating layers, J. Appl. Polym. Sci 46 (1992) 1927–1938.
[18] U. Beuscher, C.H. Gooding, The influence of the porous support layer of composite membranes on the separation of binary gas mixtures, J. Membr. Sci. 152 (1999) 99–116.
[19] X. Ding, Y. Cao, H. Zhao, L. Wang, Q. Yuan, Fabrication of high performance matrimid/polysulfone dual-layer hollow fiber membranes for O_2/N_2 separation, J. Membr. Sci. 323 (2008) 352–361.
[20] F. Hamad, K.C. Khulbe, T. Matsuura, Comparison of gas separation performance and morphology of homogeneous and composite PPO membranes, J. Membr. Sci. 256 (2005) 29–37.
[21] W. Yoshida, Y. Cohen, Ceramic-supported polymer membranes for pervaporation of binary organic/organic mixtures, J. Membr. Sci. 213 (2003) 145–157.
[22] L.M. van der Haar, H. Verweij, Homogeneous porous perovskite supports for thin dense oxygen separation membranes, J. Membr. Sci. 180 (2000) 147–155.
[23] W. Wei, G. Qin, H. Hu, L. You, G. Chen, Preparation of supported carbon molecular sieve membrane from novolac phenol–formaldehyde resin, J. Membr. Sci. 303 (2007) 80–85.
[24] F. Huber, J. Springer, M. Muhler, Plasma Polymer Membranes from Hexafluoroethane/Hydrogen Mixtures for Separation of Oxygen and Nitrogen, J. Appl. Polym. Sci. 63 (1997) 1517–1526.
[25] X. Ma, B.K. Lin, X. Wei, J. Kniep, Y.S. Lin, Gamma-alumina supported carbon molecular sieve membrane for propylene/propane separation, Ind. Eng. Chem. Res. 52 (2013) 4297–4305.
[26] Y. Wang, Observation of α-Al_2O_3 Powder Sintering Behaviors, Department of Resources Engineering, National Cheng Kung University, Taiwan, 2002.
[27] Q. Hong, N. Shufeng, J. Xiaoluo, X. Nanping, Enhanced performance of a macroporous ceramic support for nanofiltration by using α-Al_2O_3 with narrow size distribution, Ceram. Int. 39 (2013) 2463–2471.
[28] M. Ashby, A first report on sintering diagrams, Acta Metall. 22 (1974) 275–289.
[29] A.C. Lua, J. Su, Effects of carbonisation on pore evolution and gas permeation properties of carbon membranes from Kapton polyimide, Carbon 44 (2006) 2964–2972.
[30] M. Moaddeb, W.J. Koros, Effects of colloidal silica incorporation on oxygen/nitrogen separation properties of ceramic-supported 6FDA-IPDA thin films, J. Membr. Sci. 111 (1996) 283–290.
[31] L.M. Robeson, The upper bound revisited, J. Membr. Sci. 320 (2008) 390–400.
[32] A.B. Fuertes, T.A. Centeno, Carbon molecular sieve membranes from polyetherimide, Micro. Meso. Mater. 26 (1998) 23–26.
[33] H.H. Tseng, A.K. Itta, Modification of carbon molecular sieve membrane structure by self-assisted deposition carbon segment for gas separation, J. Membr. Sci. 389 (2012) 223–233.
[34] H.H. Tseng, P.T. Shiu, Y.S. Lin, Effect of mesoporous silica modification on the structure.of hybrid carbon membrane for hydrogen separation, Int. J. Hydrog. Energy 36 (2011) 15352–15363.
[35] H.H. Tseng, K. Shih, P.T. Shiu, M.Y. Wey, Influence of support structure on the permeation behavior of polyetherimide-derived carbon molecular sieve composite membrane, J. Membr. Sci. 405-406 (2012) 250–260.